Bosons with incommensurate potential and spin-orbit coupling

Sayak Ray,[1] Bhaskar Mukherjee,[2] Subhasis Sinha,[1] and K. Sengupta[2]
[1]*Indian Institute of Science Education and Research, Kolkata, Mohanpur, Nadia 741246, India*
[2]*Theoretical Physics Department, Indian Association for the Cultivation of Science, Jadavpur, Kolkata-700032, India*
(Received 10 March 2017; revised manuscript received 23 June 2017; published 4 August 2017)

We chart out the phases of ultracold "spin-half" bosons in a one-dimensional optical lattice in the presence of Aubry-André (AA) potential and with spin-orbit (SO) and Raman couplings. We investigate the superfluid (SF) and localized phases and demonstrate the existence of density wave phase for nearest-neighbor interaction (NNI) between the bosons. We show that the presence of SO coupling and AA potential leads to a spin-split momentum distribution of the bosons in the localized phase near the boundary with the SF phase, which can act as a signature of the SF-localized phase transition. We also obtain the level statistics of the bosons in the superfluid phase with finite NNI and demonstrate its change from Gaussian unitary ensemble (GUE) to Gaussian orthogonal ensemble (GOE) as a function of the Raman coupling. We discuss experiments which can test our theory.

DOI: 10.1103/PhysRevA.96.023607

I. INTRODUCTION

The study of localization phenomena in correlated systems has regained a new interest recently in the context of many-body localization (MBL) [1,2]. Ultracold atoms in optical lattices, which act as emulators of strongly correlated model Hamiltonians [3], can serve as test beds for such phenomena [4,5]. In this context, systems with quasiperiodic potentials, which have posed several interesting theoretical challenges over many decades [6–8], turn out to be particularly relevant. A model Hamiltonian describing such a quasiperiodic system is the well-known Aubry-André (AA) model [9], which, unlike the Anderson model, exhibits localization transition in one dimension [9,10]. This property of the AA model has generated an impetus to study MBL [11,12]. Moreover, experimental realization of the AA model in bichromatic optical lattice has led to observation of localization of both the light [13] and ultracold matter wave [14,15].

In the recent past, extensive research on the Bose-Hubbard (BH) model using ultracold bosonic atoms in optical lattices paved the way for studying the effect of interactions on localization phenomenon [16] leading to possible glassy phases [17–20]. In addition, intense theoretical studies have also been carried out on the BH model in the presence of Abelian and non-Abelian gauge fields; such gauge fields have been experimentally realized in atom-laser systems [21,22]. Such systems allow for observation of several exciting phenomena [23–25]; most interestingly, they enable us to study strongly interacting bosons in the presence of tunable spin-orbit (SO) coupling [26–30]. Furthermore, recent studies have predicted interesting phases of a SO coupled dilute weakly interacting Bose gas in the presence of periodic or quasiperiodic potentials [31–33]. Moreover the effect of SO interaction on the single-particle properties of disordered noninteracting electronic system has led to several recent studies [34–36]. The realization of the AA model in bichromatic lattice and the creation of SO interactions for ultracold bosons therefore provides a unique opportunity to study localization phenomenon induced by the AA potential in the presence of tunable SO interactions in one dimension; moreover it allows us to study the effect of strong interactions in such systems which, to the best of our knowledge, has not been studied before.

In this work, we study a two-species Bose-Hubbard model coupled by Raman frequency Ω, in the presence of AA potential and SO coupling and show that such a system leads to several features which appear only in the presence of both the AA potential and the SO coupling. The Hamiltonian of such a Bose Hubbard model is given by

$$\hat{H} = -J\sum_{l,\sigma}\left(\hat{b}^{\dagger}_{l,\sigma}e^{iq\hat{\sigma}_z}\hat{b}_{l+1,\sigma} + \text{H.c.}\right) + \frac{1}{2}\sum_{l,l'}\mathcal{V}_{l,l'}\hat{n}_l\hat{n}_{l'} + \lambda\sum_{l,\sigma}\cos(2\pi\beta l)\hat{n}_{l,\sigma} + \Omega\sum_{l,\sigma}\hat{b}^{\dagger}_{l,\sigma}\hat{b}_{l,\bar{\sigma}}, \quad (1)$$

where, $\hat{b}^{\dagger}_{l,\sigma}$ and $\hat{n}_{l\sigma} = \hat{b}^{\dagger}_{l,\sigma}\hat{b}_{l,\sigma}$ are the creation and the density operator of the bosons of (pseudo)spin σ at the lattice site l, $\hat{n}_l = \sum_\sigma \hat{n}_{l\sigma}$, $\bar{\sigma} = \downarrow (\uparrow)$ for $\sigma = \uparrow (\downarrow)$, J is the hopping strength, q is the SO coupling strength, Ω is the Raman frequency, $\hat{\sigma}_{x,y,z}$ are the usual Pauli spin matrices, and λ and β denotes the strength and period of the quasiperiodic potential, respectively. In the rest of the paper we consider nearest neighbor and on-site interactions with coupling strengths: $V = \mathcal{V}_{l,l+1}$ and $U = \mathcal{V}_{l,l}$, respectively, and we choose $\beta = (\sqrt{5}-1)/2$ which is a Diophantine number. In what follows, we shall scale all energies in units of J.

The central results of our study are as follows. First, we chart out the phase diagram of one-dimensional (1D) ultracold bosons in an optical lattice and demonstrate the existence of density wave (DW), superfluid (SF), and localized phases and study the transition (or more accurately crossovers for finite-sized systems) between these phases. Second, we show that for sufficiently high Ω, the bosons in the presence of both the AA potential and the SO coupling exhibits a spin-split momentum distribution in the localized phase, near the boundary with the SF phase, irrespective of the strength of their interaction. Such a splitting can therefore serve as a signature of this transition. We note that this spin splitting does not occur in the absence of either the AA potential or the SO coupling. Third, we study the level statistics of the bosons in the strongly interacting regime, where the presence of the AA potential and Raman coupling Ω between the spins play a crucial role in changing the spectral statistics between different universality classes of random matrix theory (RMT). Apart from Poissonian level

 ©2017 American Physical Society

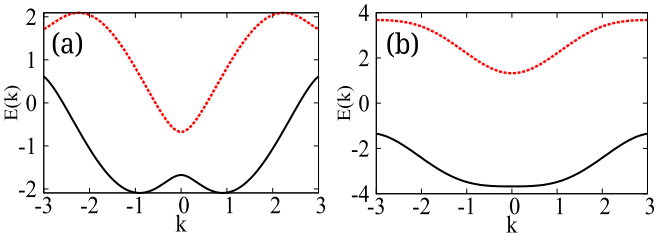

FIG. 1. Energy dispersion for (a) $\Omega < \Omega_c$ and (b) $\Omega > \Omega_c$. All energies are scaled in units of J and all momenta are scaled with inverse lattice spacing a_0^{-1}.

spacing distribution in the localized regime, we find that the level statistics change continually from GUE ($\Omega = 0$) to GOE as a function of Ω. We identify the additional symmetry at the $\Omega = 0$ point which is behind this change. Finally, we discuss possible experiments which can test our theory.

The organization of the rest of the work is as follows. In Sec. II, we investigate the properties of the system in the noninteracting limit. This is followed by analogous studies on hard-core bosons with finite nearest-neighbor interaction in Sec. III. Next, in Sec. IV, we study the spectral statistics of the bosons. This is followed by a study of nonequilibrium dynamics of the bosons in the strongly coupled regime in Sec. V. Finally, we summarize our results, discuss relevant experiments, and conclude in Sec. VI. We also provide a discussion on momentum distribution of weakly coupled bosons in the appendix.

II. NONINTERACTING BOSONS

In this section, we analyze the single-particle properties of this Hamiltonian [Eq. (1)] by setting $U = V = 0$. For $\lambda = 0$, this reduces to a system of SO coupled bosonic particles with a 2×2 matrix in the momentum representation as

$$H_{\rm so} = \sum_{k,\sigma} \psi_k^\dagger \begin{pmatrix} -2\cos(k+q) & \Omega \\ \Omega & -2\cos(k-q) \end{pmatrix} \psi_k, \quad (2)$$

where $\psi_k = (b_{k\uparrow}, b_{k\downarrow})^T$ is the two-component boson field. The single-particle energy spectrum for $H_{\rm so}$ is

$$E_k^{\pm} = -2\cos k \cos q \pm 2[\sin^2 k \sin^2 q + \Omega^2/4]^{1/2}, \quad (3)$$

and the eigenstates are given by

$$\psi_k^{\pm} = (\cos(\theta_k - \pi/4 \mp \pi/4), \sin(\theta_k - \pi/4 \mp \pi/4))^T,$$
$$\cos\theta_k = [1/2 + [4 + \Omega^2/(\sin^2 k \sin^2 q)]^{-1/2}]^{1/2}. \quad (4)$$

From the lower branch of the energy dispersion E_k^-, we find that there exists a critical value Ω_c below which the ground state is doubly degenerate; this critical Raman coupling is given by

$$\Omega_c = 2\sin q \tan q. \quad (5)$$

For $\Omega < \Omega_c$, the minima of the energy dispersion shifts to $\pm k_0$, where

$$k_0 = \pm\cos^{-1}[\cos q\sqrt{1 + \Omega^2/(4\sin^2 q)}]. \quad (6)$$

This is illustrated in Fig. 1. These doubly degenerate ground states are related by $\psi_{-k} = \hat{\sigma}_z \hat{\mathcal{T}} \psi_k$, where $\hat{\mathcal{T}} = -i\hat{\sigma}_y \hat{\mathcal{C}}$ is the time reversal symmetry (TRS) operator, $\hat{\mathcal{C}}$ is the complex conjugation operator, and $\hat{\sigma}_{x,y,z}$ are the usual Pauli spin matrices. We note here that the effective mass (or the band mass) of the bosons is thus given by $m^{*-1} = \partial_k^2 E_k^-|_{k=k_0}$. For $\Omega > \Omega_c$, the expression of m^* can be written as

$$m^{*-1}_{\Omega>\Omega_c} \equiv m^{*-1}_{>} = \left(\frac{\partial^2 E_k^-}{\partial k^2}\right)_{k=0} = (1 - \Omega_c/\Omega)\cos q. \quad (7)$$

In the absence of disorder, the superfluid fraction (SFF), given by $\partial^2 E_g/\partial\theta^2$, thus turns out to be the inverse of the boson effective mass. Thus m^{*-1} captures the behavior of the SFF obtained numerically as a function of Ω [see Fig. 2(a)]; this situation is similar to that obtained in the continuum limit [37].

For $q = \Omega = 0$, the above Hamiltonian is reduced to a two-component AA model which undergoes a localization transition above a critical coupling strength $\lambda_c = 2$. For two extreme regimes $q \neq 0, \Omega = 0$ (pure SO coupling) and $q = 0, \Omega \neq 0$ (strong Raman coupling) the single-particle Hamiltonian preserves the self-duality at $\lambda_c = 2$ and all states are localized above λ_c. Similar studies on duality for quasiperiodic systems in the absence of spin-orbit coupling is done in Refs. [34,35]. To study localization transition in the intermediate regime with $q \neq 0, \Omega \neq 0$, we numerically diagonalize the single-particle Hamiltonian to obtain the ground state and the excitation spectrum. Since the duality does not hold in this regime a mobility edge appears and energy dependent localization occurs for eigenstates [34]. We focus on the localization transition of the ground state in the presence of SO interaction and the variation of the critical disorder strength λ_c on Raman coupling. We locate the change from the SF to the localized phase in two ways. First, we measure the superfluid fraction (SFF) by applying a phase twist [38] $\theta \ll \pi$ at the boundary. In the presence of such a twist $J_{l,l+1} \to Je^{i\theta/N_s}$ [Eq. (1)]. The SFF can then be computed as [20]

$$f_s = N_s^2(E[\theta] - E[0])/(N_p\theta^2), \quad (8)$$

where $E[\theta]$ is the ground-state energy in the presence of twist, and $N_s(N_p)$ is the number of sites (particles).

The second measure of localization is the inverse participation ratio (IPR) of the ground-state wave function defined as

$$I = \sum_l (|\psi_{l,\uparrow}|^2 + |\psi_{l,\downarrow}|^2)^2, \quad (9)$$

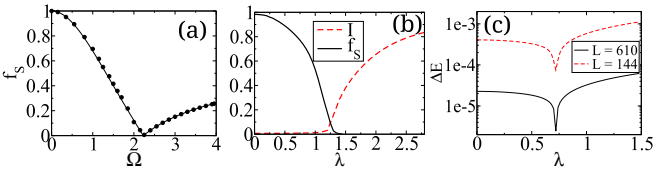

FIG. 2. (a) Superfluid fraction as a function of Ω for $\lambda = 0$. Solid line represents the SFF obtained analytically from the effective mass calculation. (b) SFF and IPR of the ground state is plotted as a function of λ for $\Omega = 0.2$. (c) Energy gap between ground state and first excited state as a function of λ for $\Omega = 3.5$. All energies are scaled in units of J and all momenta are scaled with inverse lattice spacing a_0^{-1}.

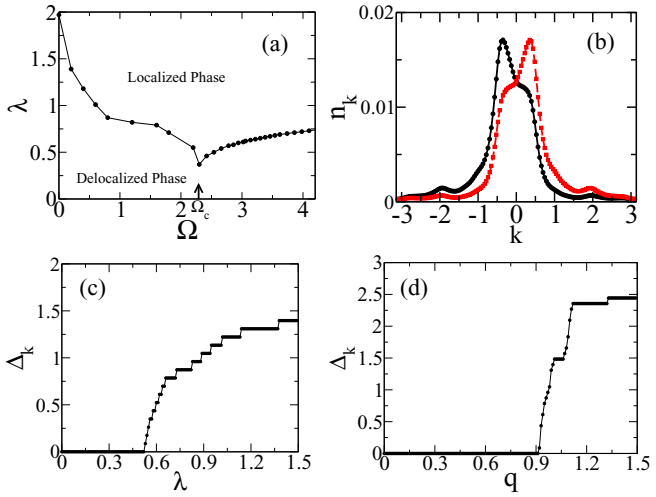

FIG. 3. (a) Phase diagram is shown in the Ω-λ plane. (b) Momentum distribution in the delocalized phase is shown for $\Omega = 2.5$, $\lambda = 0.65$. Solid (dashed) curves correspond to the up (down) spin. (c)and (d) Δ_k as a function of λ for $q = 0.3\pi$ and as a function of q for $\lambda = 0.65$ is shown. For both the plots we set $\Omega = 2.5$. All energies are scaled in units of J and all momenta are scaled with inverse lattice spacing a_0^{-1}.

where $|\psi_{l,\sigma}|^2$ is the boson density of spin σ at site l. As expected, we find that SFF decreases and the IPR increases with increasing λ around the transition [see Fig. 2(b)].

The phase diagram obtained from these computations is shown in Fig. 3(a) in the λ−Ω plane for $q = 0.3\pi$. We note that λ_c decreases from its self-dual value ∼2 for $q \neq 0$ and shows a dip at Ω_c, which demarcates the delocalized phase in two regimes. Below Ω_c the degeneracy of the ground state is lifted by the quasiperiodic potential; however the ground state has a net momentum and s_z polarization. For $\Omega > \Omega_c$, the ground-state wave function is spin polarized along $\hat{x}$ and has vanishing net momentum. The behavior of λ_c with Ω can be understood from the enhancement of effective mass of bosons in the lower branch $m^{*-1} = \partial^2 E_k^-/\partial k^2|_{k=k_0}$ due to the combined effect of SO and Raman couplings. This in turn reduces the effective hopping strength $J_{\rm eff} = J/m^*$ of the underlying AA model for which the critical strength for the localization transition can be estimated as $\lambda_c \sim 2J_{\rm eff} \sim 2/m^*$. We note that the idea of m^* also quantitatively explains the variation of SFF with Ω for $\lambda = 0$ and that SFF decreases and the IPR increases with increasing λ around the transition as expected.

To elucidate the role of the AA potential and the SO coupling in the transition, we compute the spin-resolved momentum distribution defined as

$$n_{k\sigma} = \sum_{l,l'} \exp\{ik(l-l')\}\langle c_{l\sigma}^\dagger c_{l'\sigma}\rangle/N_s, \qquad (10)$$

where $k = 2\pi m/N_s$, with $m \in [-N_s/2, (N_s-1)/2]$. For $\Omega > \Omega_c$, both $n_{k\uparrow}$ and $n_{k\downarrow}$ is peaked at $k = 0$ in the delocalized phase as seen for standard superfluids. In contrast, in the localized regime near the transition, $n_{k\sigma}$ becomes spin dependent and is peaked at $k = k_\sigma^{\max} \neq 0$ preserving the symmetry $n_\uparrow(k) = n_\downarrow(-k)$ [see Fig. 3(b)]. The splitting of these peaks are given

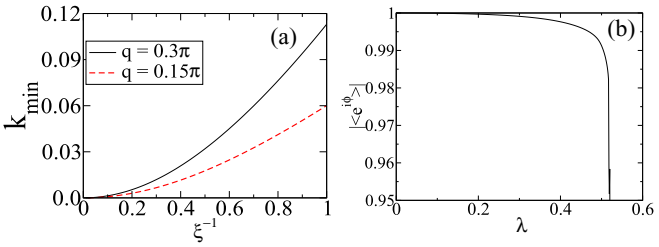

FIG. 4. (a) $k_{\rm min}$ as a function of ξ^{-1} is plotted for $\Omega = 3$. (b) $|\langle e^{i\phi}\rangle|$ as a function of λ has been plotted for noninteracting bosons for $\Omega = 2.5$ and $q = 0.3\pi$. All energies are scaled in units of J and all momenta are scaled with inverse lattice spacing a_0^{-1}.

by $\Delta_{k_\sigma^{\max}} = k_\uparrow^{\max} - k_\downarrow^{\max} \sim q$ leading to the conclusion that the split in $n_{k\sigma}$ arises from a finite SO coupling. As shown in Figs. 3(c) and 3(d), $\Delta_{k_\sigma^{\max}}$ vanishes for either $q = 0$ or $\lambda = 0$; this shows the necessity of both the AA potential and the SO coupling for the peak splitting.

The effect of spin-split momentum distribution of the localized wave function in the regime $\Omega > \Omega_c$ arises due to the interplay between the SO interaction and Raman coupling and can be qualitatively understood from a simple variational calculation. To this end, we construct the variational wave function describing the localized bosons given by

$$\psi_l = \mathcal{N} e^{-|l|/\xi}\begin{pmatrix} e^{ikl} \\ -e^{-ikl}\end{pmatrix}, \quad \mathcal{N} = \sqrt{\frac{\tanh(1/\xi)}{2}}, \qquad (11)$$

where l is the site index and ξ represents localization length which contains the effect of AA potential and the interaction. The spinor part is chosen in such a way that up (down) spin momentum distribution is peaked at $\pm k$ and for $k = 0$ it reduces to the usual form of the ground state for $\Omega > \Omega_c$. For the aforementioned wave function, the parameter k is treated as the variational parameter and we investigate its dependence on ξ and Ω. Considering the single-particle Hamiltonian of a spin-orbit (SO) coupled bosonic system in an optical lattice, the energy can be written as

$$E(k) = -\left[\frac{\cos(k-q)}{\cosh(1/\xi)} + \frac{\Omega\tanh(1/\xi)\sinh(2/\xi)}{\cosh(2/\xi)-\cos 2k}\right]. \qquad (12)$$

We minimize $E(k)$ to obtain $k_{\rm min}$ and have shown its variation as a function of ξ^{-1} in Fig. 4(a); it is evident that $k_{\rm min}$ decreases with increasing ξ and finally it vanishes in the delocalized regime, i.e., $\xi^{-1} \to 0$. We further notice for a fixed ξ the spin splitting (characterized by $k_{\rm min}$) decreases with decreasing strength of SO interaction (q) and eventually vanish for $q = 0$. This simple variational calculation elucidates how the combined effect of localization and SO interaction gives rise to the spin splitted momentum distribution in the regime $\Omega > \Omega_c$.

Finally, we relate the effect of spin splitting in momentum distribution near the localization transition with phase fluctuation of the wave function. In general, the boson wave function can be written as

$$\psi^l = \sqrt{n_0^l}\begin{pmatrix}\cos\theta^l e^{i\phi_\uparrow^l} \\ \sin\theta^l e^{i\phi_\downarrow^l}\end{pmatrix}, \qquad (13)$$

where $\phi_l = \phi^l_\uparrow - \phi^l_\downarrow$ is the phase angle of the spinor at site l. For $\Omega > \Omega_c$, we find that $\cos\theta = \sin\theta \approx 1/\sqrt{2}$ and $\phi \approx \pi$ in the delocalized phase, whereas, near localization transition due to increasing phase fluctuations, the phase angle fluctuates significantly from π at different sites. We quantify the phase fluctuation by calculating $|\langle e^{i\phi}\rangle|$, where the average is taken over all the lattice sites. In Fig. 4(b) we have shown the behavior of $|\langle e^{i\phi}\rangle|$ as a function of the disorder potential strength λ which shows that near the localization transition it decreases from 1 with increasing strength of the disorder λ. This indicates that spin diffusion is intimately related to the momentum spilling of the boson momentum distribution; both these phenomenon originates from the combined effect of AA potential and the SO coupling.

III. BOSONS WITH HARD-CORE REPULSION

In this section, we study the properties of interacting bosons with AA potential and spin-orbit coupling. First, we consider the case $V = 0$, where, at half-filling, the bosons are always in the SF phase for zero or weak AA potential. The choice of such a hardcore limit facilitates computation by imposing the constraint $n_l \leqslant 1$ at each site and allows us to perform exact diagonalization within a restricted Hilbert space of three states per site. We restrict our calculation to half-filled HC bosons, $\sum_l n_l = N_s/2$, so that we are always in the SF phase for $\lambda = V = 0$. In addition to SFF we also compute the boson condensate fraction (BCF) since BCF and SFF are quite different for strongly interacting bosons and are important for characterizing the localized phases. We construct the one-body density matrix from the ground state $|\psi_0\rangle$ given by

$$\rho(l,\sigma;l',\sigma') = \langle\psi_0|\hat{b}^\dagger_{l',\sigma'}\hat{b}_{l,\sigma}|\psi_0\rangle. \tag{14}$$

We note that the largest eigenvalue N_c of $\rho(l,\sigma;l',\sigma')$ gives the BCF $f_c = N_c/\mathrm{Tr}(\hat{\rho})$ [39].

A plot of f_s and f_c in the $\Omega-\lambda$ plane for a fixed q is shown in Figs. 5(a) and 5(b). These plots clearly indicate a regime for $\lambda > \lambda_c$ where f_s vanishes but f_c remains finite indicating a localized phase of the bosons. Although in the finite system there is no transition, the behavior of λ_c obtained from SFF is similar to that for noninteracting bosons; however, Ω_c shifts to a lower value. Near this boundary, particularly for $\Omega \leqslant \Omega_c$, there is clear indication of the Bose-glass (BG) phase with $f_s = 0$ and $f_c \neq 0$.

We have also studied the variation of SFF with coupling strength λ as shown in Fig. 6 for different numbers of lattice sites: $N = 8,10,12$. The variation of SFF with system size is not a significant deep inside the SF phase away from the crossover region to the localized phase. Also for the noninteracting AA model finite size scaling analysis of IPR has been presented in Ref. [11]. These results clearly indicate that finite size effects are not too large in the AA model. Thus we expect that the phases obtained from our analysis shall be present for larger systems. However, we note that a more sophisticated finite size scaling analysis with much larger system size is required to determine the phase boundaries and the nature of the phase transition. This is clearly beyond the scope of the exact diagonalization method that we use here.

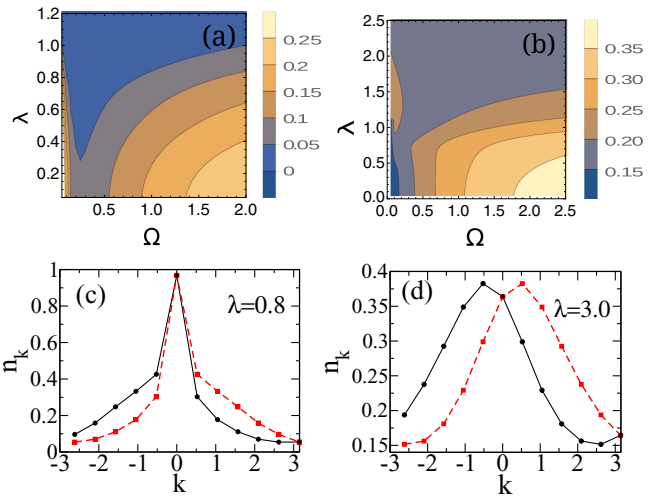

FIG. 5. (a) and (b) Color plot of the SFF f_s and the BCF f_c have been shown in the Ω-λ plane for $q = 0.3\pi$ and number of sites $N_s = 12$ at half filling. (c) and (d) Momentum distribution of spin up (down) particles are shown for $\Omega = 2.5$ by solid (dashed) lines. All energies are scaled in units of J and all momenta are scaled with inverse lattice spacing a_0^{-1}. See the text for details.

Since true phase transition is absent in finite systems, we only show the variation of the relevant order parameters without any phase boundary in the phase diagram to identify various phases and crossover between them. We would like to point out in this context that the results obtained for finite lattice size are of direct relevance with real experimental systems for which the typical lattice sites are $N \leqslant 12$ [40].

Finally, we compute the $n_{k\sigma}$ of the hardcore bosons for $V = 0$. As shown in Figs. 5(c) and 5(d), the splitting of the spin momentum peak occurs in the localized phase and survives in the hardcore limit. We have checked that $n_{k\sigma}$ are peaked at $k = 0$ in the delocalized regime and at $k_\sigma^{\max}$ in the localized regime near the transition. Thus we find that the shift in $n_{k\sigma}$ due to the presence of a finite q survives in the presence of strong on-site interaction. Similar conclusions can be drawn

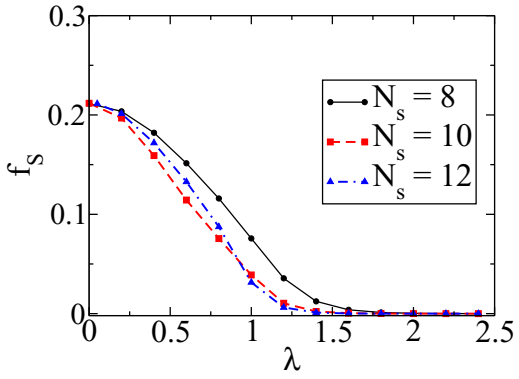

FIG. 6. Superfluid density as a function of λ for $\Omega = 1.5$, $q = 0.3\pi$ and using different system sizes at half filling as mentioned in the inset. All energies are scaled in units of J and all momenta are scaled with inverse lattice spacing a_0^{-1}.

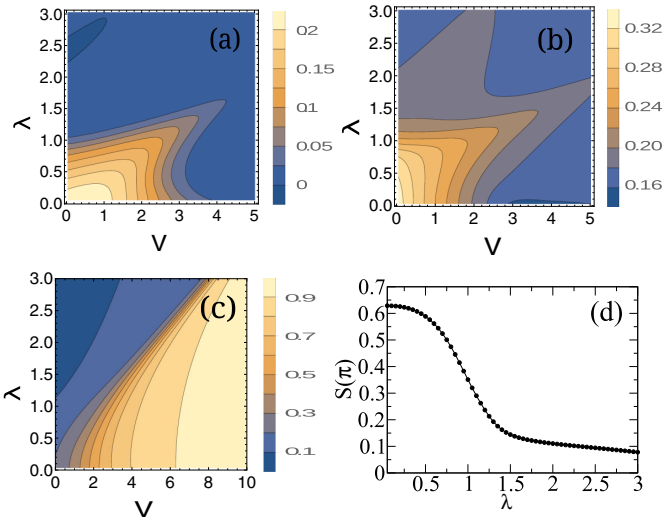

FIG. 7. Color plot of the (a) superfluid density, (b) condensate fraction, and (c) $S(\pi)$ for bosons at half filling with $N_s = 12$ as a function of V and λ for $\Omega = 1.5$ and $q = 0.3\pi$. (d) $S(\pi)$ as a function of λ for $V = 2.5$. All energies are scaled in units of J and all momenta are scaled with inverse lattice spacing a_0^{-1}. See the text for details.

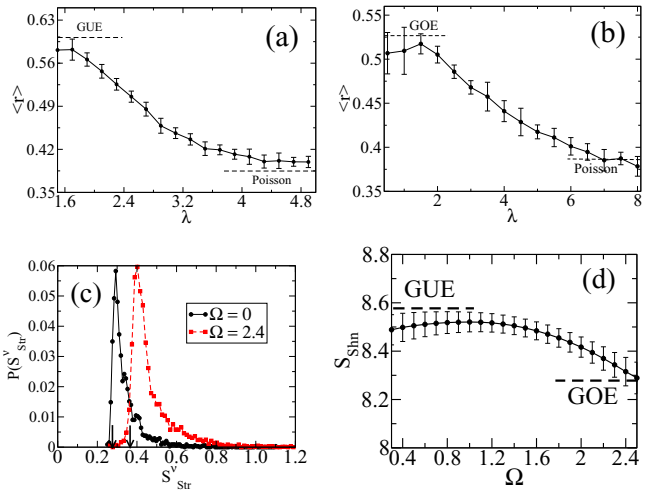

FIG. 8. (a) and (b) $\langle r \rangle$ (averaged over 20 disorder realizations) as a function of λ for $\Omega = 0$ and $\Omega = 2$, respectively. (c) Distribution of $S_\nu^{\rm Str}$ of different eigenmodes (ν) is shown for $\lambda = 0.8$. Average $S_\nu^{\rm Shn}$ as a function of Ω is shown in (d) for $\lambda = 0.8$. We set $V = 0.9$ for all the plots. All energies are scaled in units of J and all momenta are scaled with inverse lattice spacing a_0^{-1}.

for weakly interacting bosons for which $U/J \ll 1$; this has been detailed in Appendix A.

Next we turn on a finite V for the hardcore bosons and obtain the phase diagram by computing SFF and BCF as a function of V/J and λ/J for a fixed q and Ω [see Figs. 7(a) and 7(b)]. For small V we find that an increase of λ leads to a depletion of superfluid density keeping the condensate fraction finite indicating a finite-size crossover from an SF to a localized phase. Similarly for a fixed small λ, an increase in V leads to an analogous depletion of superfluid density; this indicates the onset of the DW phase with broken translational symmetry. For $\lambda = \Omega = 0$, Eq. (1) reduces to the well-studied XXZ model which exhibits the SF to DW transition at $V/J = 1$ [41]. Similarly for the SF-DW transition at small λ, a first-order transition is expected since the DW state breaks translational invariance while the SF states breaks $U(1)$ gauge symmetry.

The phase diagram of the bosons in the large V/J regime as a function of λ cannot be completely understood from Figs. 7(a) and 7(b) since $\rho_s = 0$ for all λ in this regime. To have an understanding of the nature of the boson phase with increasing λ, we study the structure factor given by

$$S(k) = 4 \sum_{l,l'=1}^{N_s} e^{ik(l-l')} \langle \hat{n}_l \hat{n}_{l'} \rangle / N_s. \tag{15}$$

We first note that in the limit $\lambda/J << 1$ the ground state forms a DW leading to $S(\pi) \simeq 1$ and $S(k) \simeq 0$ for $k \neq \pi$ [42]. This DW state is expected to melt with increasing λ leading to a vanishing of peak of $S(k)$ at $k = \pi$. A plot of $S(\pi)$ in the $\lambda - V$ plane, shown in Fig. 7(c), indicates the melting with increasing λ. The dynamical signature of such melting may be obtained by studying boson dynamics following quench of λ across its melting value. We shall present our results on this issue in Sec. V.

IV. SPECTRAL STATISTICS OF BOSONS

In this section, we show that the present model with $V \neq 0$ hosts a change of spectral statistics from GUE-GOE in the superfluid phase at finite λ. To this end, we first note that for $\Omega = 0$, $[\hat{H}, \hat{S}_z] = 0$, and the boson ground state lies in the $S_z^{\rm total} = N_s/2$ sector. However, for states within this sector, one does not have TRS since $[\hat{H}, \hat{\mathcal{T}}] \neq 0$ for a fixed S_z sector. Thus for $\Omega = 0$ with a fixed $S_z^{\rm max} \neq 0$ sector, one has $[\hat{H}, \hat{S}_z \hat{\mathcal{T}}] \neq 0$. In contrast for $\Omega \neq 0$, it is easy to see using Eq. (1), $[\hat{H}, \hat{S}_z \hat{\mathcal{T}}] = 0$. The latter symmetry is a consequence of invariance of $\hat{H}$ under TRS followed by a π rotation in spin space about the z axis. The presence of this additional symmetry leads to GOE to GUE crossover as Ω is turned on and increased [36,43,44].

To show this, we first calculate the level spacing ratio given by [11,45]

$$r_\nu = \min(\delta_{\nu+1}, \delta_\nu)/\max(\delta_{\nu+1}, \delta_\nu), \tag{16}$$

where $\delta_\nu = E_{\nu+1} - E_\nu$, and E_ν is the $\nu^{\rm th}$ energy eigenvalue. We compute the quantity $\langle r \rangle = \sum_\nu r_\nu / \mathcal{N}$, where $\mathcal{N}$ is the total number of levels. For $\Omega = 0$, working with the energy levels in the maximal S_z sector, we find that $\langle r \rangle$ shows a crossover from its GUE value of $\approx$0.58 to that for Poisson statistics $\approx$0.38 with increasing λ [see Fig. 8(a)]. In contrast, for large $\Omega = 2$, a similar analysis shows that $\langle r \rangle$ crosses over from its GOE value of $\approx$0.527 to Poisson with increasing λ [see Fig. 8(b)].

In finite-sized systems with no strict symmetry breaking, the level statistics cannot be captured for small but finite Ω values. We therefore concentrate on the variation of the Shannon and structural entropy for studying the crossover between GUE-GOE statistics. The eigenvector corresponding to the $\nu^{\rm th}$ eigenmode can be written as

$$|\Phi_\nu\rangle = \sum_\chi c_\nu^\chi |\chi\rangle, \tag{17}$$

where $|\chi\rangle$ are the basis states. The corresponding Shannon entropy is given by

$$S_\nu^{\rm Shn} = -\sum_\chi |c_\nu^\chi|^2 \ln |c_\nu^\chi|^2. \quad (18)$$

It is well known that $S^{\rm Shn} = \sum_\nu S_\nu^{\rm Shn}$ has the value $S_{\rm GOE}^{\rm Shn} = \Psi(N/2+1) - \Psi(3/2)$ for GOE and $S_{\rm GUE}^{\rm Shn} = \Psi(N+1) - \Psi(2)$ for GUE [46,47]. Here Ψ is the Digamma function and N is the system dimension. The structural entropy for the νth eigenmode is defined as

$$S_\nu^{\rm Str} = S_\nu^{\rm Shn} - \ln \xi_\nu, \quad (19)$$

where ξ_ν is the IPR corresponding to the νth eigenmode. It is known that $S_\nu^{\rm Str} \approx 0.37(0.27)$ for GOE(GUE) [47,48]. In Fig. 8(c), we have plotted the distribution of $S_\nu^{\rm Str}$ showing that the peak of the distribution shifts from in the delocalized regime its GUE value (≈0.27) to its GOE value (≈0.37) as Ω is changed from 0.6 to 2.0. In Fig. 8(d), we plot the variation of $S_\nu^{\rm Shn}$ showing a smooth crossover from its value for GUE to that for GOE with increasing Ω.

V. NONEQUILIBRIUM DYNAMICS

To elucidate the localization transition of the HCB, we now look into the nonequilibrium dynamics of the bosons. We start from the density wave state at $\lambda = 0$ denoted by $|\psi(0)\rangle$. Next we quench λ to a finite value λ_f so that the system Hamiltonian after the quench is given by $H[\lambda_f]$. Let us denote the eigenfunctions and eigenvalues of $H[\lambda_f]$ as $|m\rangle$ and ϵ_m, respectively. The time-evolved wave function $|\psi(t)\rangle$ at any instant of time t after the quench can be obtained by solving the Schrodinger equation $i\hbar\partial_t|\psi(t)\rangle = H[\lambda_f]|\psi(t)\rangle$ and is given by

$$|\psi(t)\rangle = \sum_m c_m e^{-i\epsilon_m t/\hbar}|m\rangle, \quad c_m = \langle m|\psi(0)\rangle. \quad (20)$$

The expectation value of any operator $O(t)$ can be obtained from $|\psi(t)\rangle$ as

$$\langle\psi(t)|O|\psi(t)\rangle = \sum_{m,n} c_m^* c_n e^{i(\epsilon_m-\epsilon_n)t/\hbar}\langle m|O|n\rangle. \quad (21)$$

Using Eq. (21), we calculate the time evolution of the imbalance factor which is defined as

$$\mathcal{I} = \frac{N_o - N_e}{N_{\rm tot}}, \quad (22)$$

where, $N_{o[e]} = \langle\psi(t)|\sum_{i\in{\rm odd[even]sites}}\hat{b}_i^\dagger\hat{b}_i|\psi(t)\rangle$ and $N_{\rm tot} = N_o + N_e$. Note that at $t = 0$, we have density wave state with $\mathcal{I} = 1$ and it approaches zero for a delocalized state. In Fig. 9(a) we have shown the time evolution of $\mathcal{I}(t)$ for the up spin species (the same feature can be observed for the down spin species as well) for different λ values. We note that for small λ which corresponds to the delocalized regime, $\mathcal{I}$ vanishes to zero with time showing the ergodic dynamics in that regime, whereas for larger λ value which corresponds to the localized regime, $\mathcal{I}$ doesn't vanish and saturates to some positive value which indicates the nonergodic regime and the density wave ordering is retained in the course of time evolution. In Fig. 9(b) the final density distribution after the time evolution has been shown for different values of λ.

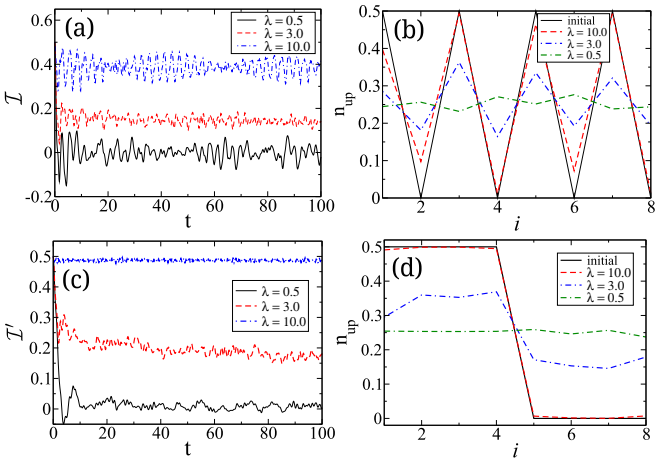

FIG. 9. The time evolution of the imbalance factor for up spin species has been shown starting from two initial states (a) density wave and (c) bosons loaded in the left half of the lattice for different values of the disorder strength λ. The final up spin density distribution at the end of the time evolution for the same λ's are shown for the two types of initial states in (b) and (d), respectively. The other parameters are $\Omega = 2$, $q = 0.3\pi$, and $V = 0$. All times are measured in units of $\hbar/J$, energies in units of J, and momenta in units of a_0^{-1}.

We repeated the same numerical experiment starting from a different initial state where the atoms are loaded on one-half of the lattice and study the imbalance factor $\mathcal{I}' = (N_l - N_r)/N_{\rm tot}$ as a function of time N_l and N_r being the total number density of bosons at the left and the right halves of the lattice, respectively. In Figs. 9(c) and 9(d) we have plotted the time evolution of the imbalance factor and the final density distribution of the up spin species for different values of the disorder strength.

Thus we find that nonequilibrium dynamics in such bosons systems can serve as a clear indicator of the localized phase. Such experiments have been carried out in the context of MBL physics on ultracold atom systems in Refs. [4,49].

VI. DISCUSSION

In this work we have analyzed the interplay between SO interaction, Raman coupling, and AA potential on the localization phenomena of strongly correlated ultracold pseudo-"spin-half" bosons in one dimension. From the superfluid fraction and condensate fraction we identified the possible phases of the hard core bosons. Apart from the superfluid and localized phase a Bose glass (BG) phase with $f_s = 0$ and $f_c \neq 0$ can exist in a large region in the phase diagram particularly for small Ω. For sufficiently large nearest neighbor interaction ($V/\lambda \gg 1$) an additional DW phase is formed which is characterized by the peak in the structure factor $S(k)$ at $k = \pi$. For small hopping strength, the melting of the density wave occurs by increasing the strength of the quasiperiodic potential resulting in the vanishing of the peak of the structure factor at $k = \pi$. The basic features of the localization transition can be understood qualitatively by analyzing the noninteracting model. Such a system exhibits the localization transition at the self-dual point $\lambda_c = 2$ either in the absence of Raman coupling Ω or for vanishing SO interaction (in the limit $q/\Omega \ll 1$).

In contrast when both the couplings are present, localization transition occurs at $\lambda_c < 2$. The variation of λ_c with Ω exhibits a minimum at the critical Raman coupling Ω_c where the nature of the ground state changes for the pure SO coupled system. We note that such a behavior of λ_c as a function of Ω resembles the dependence of the effective mass of the bosons on Ω leading to a simplified picture of bosons in the AA potential with an effective hopping strength $J_{\rm eff} \approx m^{*-1}$.

Apart from a rich phase diagram, our analysis shows that in a system of 1D ultracold bosons in an optical lattice the interplay between SO interaction, Raman coupling, and AA potential leads to the splitting in the spin-resolved momentum distribution. Above Ω_c, such a split happens only when both λ, $q \neq 0$ and may serve as an indicator of the localization transition. The experimental verification of this splitting would involve preparing a system of bosons with SO coupling [22] in the presence of a 1D bichromatic lattice to model AA potential [14]; finally the spin-resolved momentum distribution of these bosons can be measured by the usual Stern-Gerlach technique [50]. Our prediction is that such an experiment would observe a spin-split momentum distribution near the localization transition which increases with increasing λ or q. We note that typically experiments are done with finite lattice sites $N_s \sim 12$ [40]; thus our numerical results are expected to be of direct relevance for experimental systems.

We have also shown that the spectral statistics of the present model follows Poissonian distribution for large λ indicating localization and hosts a GUE-GOE crossover as a function of Ω in the delocalized regime. We note that this is an experimentally accessible model which can exhibit the transition of spectral statistics between two universality classes of RMT by tuning a physical parameter Ω. The localized and delocalized phases can also be identified by computing the imbalance factor from the nonequilibrium dynamics of the hard core bosons. In the presence of a finite λ starting from an initial DW phase we performed exact diagonalization to study the evolution of the imbalance factor which vanishes gradually with time in the delocalized phase whereas it saturates to a finite value in the localized regime. In recent experiments [4,49] on ultracold bosons such a dynamical characterization has been demonstrated and can easily be tested for our model as well.

In conclusion, we have studied a system of ultracold bosons in the presence of the AA potential and spin-orbit coupling. We have charted out the various phases of the system, demonstrated a spin-dependent split in the momentum distribution function of these bosons, and unraveled a change in the spectral statistics of the bosons from GUE to GOE. In particular, the splitting of the spin-resolved momentum distribution for $\Omega > \Omega_c$ and the change in spectral statistics from GUE to GOE by tuning the Raman coupling are the two features that we unearth; of these, the first one is expected to be easily verifiable in future experiments. We have also pointed out an experimentally verifiable dynamical signature of the localized phases in these systems.

ACKNOWLEDGMENTS

B.M. thanks S. Mukherjee and A. Dutta for useful discussion. We also thank R. Islam for discussion.

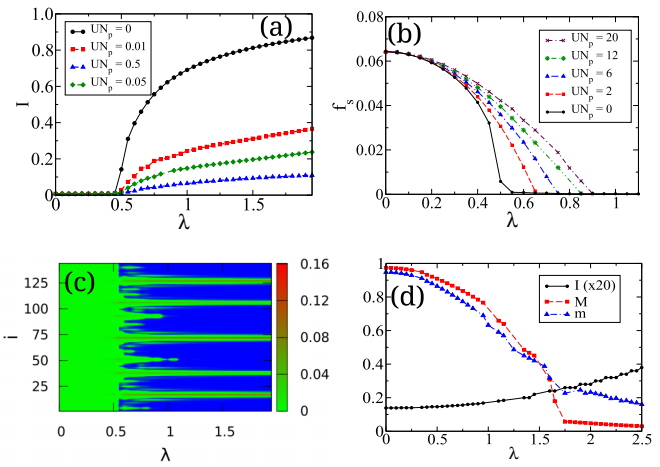

FIG. 10. The IPR and SFF have been shown as a function of λ for $\Omega = 2.5$ and for different interaction strength UN_p in (a) and (b), respectively. The spatial distribution of the ground-state density has been shown for $UN_p = 0.5$, $\Omega = 2.5$ in (c). IPR, the order parameter m, and the total magnetization M as a function of λ for $UN_p = 20$ and $\Omega = 0.3$ are shown in (d). We set $N_p = 200$ and $N_s = 144$ for all the plots. All energies are scaled in units of J.

APPENDIX: LOCALIZATION OF WEAKLY INTERACTING BOSONS

In the Appendix, we study the weakly interacting limit, i.e., for $U/J \ll 1$ and $V = 0$ of the bosons. To this end, replace the quantum field operator $\hat{b}_{l,\sigma}$ by the classical field operator $\psi_{l,\sigma}$ assuming the existence of a 1D quasicondensate [51]. By minimizing the energy functional calculated thereby, we obtain the discrete nonlinear Schrödinger (DNLS) equation for the condensate wave function $\psi_{l,\sigma}$ given by

$$
\begin{aligned}
&-(\psi_{l+1,\uparrow}e^{iq} + \psi_{l-1,\uparrow}e^{-iq}) + \lambda\cos(2\pi\beta l)\psi_{l,\uparrow} \\
&+\Omega\psi_{l,\downarrow} + U(|\psi_{l,\uparrow}|^2 + |\psi_{l,\downarrow}|^2)\psi_{l,\uparrow} = \mu\psi_{l,\uparrow} \\
&-(\psi_{l+1,\downarrow}e^{-iq} + \psi_{l-1,\downarrow}e^{iq}) + \lambda\cos(2\pi\beta l)\psi_{l,\downarrow} \\
&+\Omega\psi_{l,\uparrow} + U(|\psi_{l,\uparrow}|^2 + |\psi_{l,\downarrow}|^2)\psi_{l,\downarrow} = \mu\psi_{l,\downarrow},
\end{aligned}
$$

where μ is the chemical potential. We then obtain the ground-state wave function $\psi_{l\sigma}$ numerically and use it to compute all relevant quantities such as IPR and f_s. In what follows we have shown the results of such a numerical study which are shown in Fig. 10.

In Fig. 10(a) we plot the ground-state IPR as a function of λ for different interaction strength UN_p/J. We see that on increasing λ beyond the localization transition, the growth of IPR decreases. This is due to the fact that the ground-state wave function becomes multisite localized due to weak repulsive interaction [see Fig. 10(c)]. We further calculate the superfluid fraction which vanishes in the localized phase as depicted in Fig. 10(b).

To gain a better understanding of the localization transition, we further study the spin-resolved momentum distribution of bosons in the regime $\Omega < \Omega_c$. In contrast to the noninteracting case, the superfluid with finite U chooses one of the two symmetry broken states with spins polarized along the z axis [28]. As a result the momentum distribution corresponding

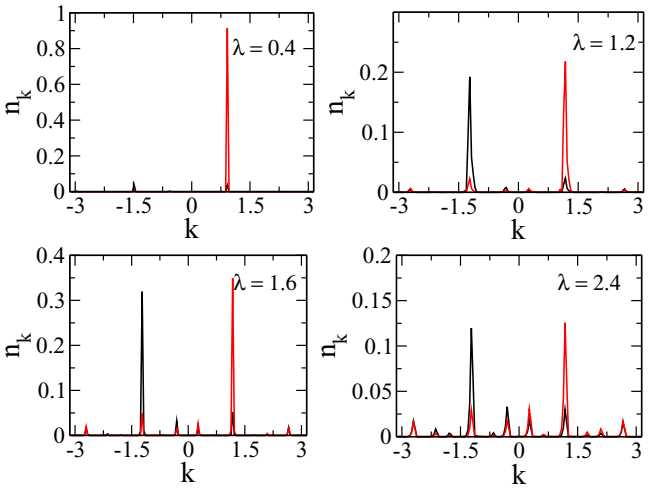

FIG. 11. Momentum distribution with increasing disorder strength λ for $\Omega = 0.5$ and $UN_p = 20$. All energies are scaled in units of J and all momenta are scaled with inverse lattice spacing a_0^{-1}.

to the spin polarization of the ground state becomes highly peaked at the nonvanishing momentum of the ground state as depicted in Fig. 11(a). With increasing disorder strength, other momentum modes get gradually occupied and spin-momentum distributions are peaked at equal and opposite momentum with a net spin polarization indicating symmetry breaking (see Fig. 11). Finally in the localized phase,

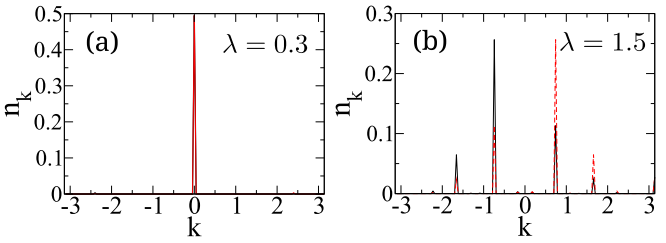

FIG. 12. (a) and (b) Momentum distribution for up(down) spin is shown in the solid(dashed) line with increasing disorder strength λ. Other parameters are $\Omega = 2.5$ and $UN_p = 10$. All energies are scaled in units of J and all momenta are scaled with inverse lattice spacing a_0^{-1}.

the momentum distributions become symmetric and peaked around finite momentum with $n_{k,\uparrow} = n_{-k,\downarrow}$. To verify this we plot the order parameter $m = \sum_k (n_{k,\uparrow} - n_{-k,\downarrow})^2$ and the total magnetization $M = \sum_k (n_{k,\uparrow} - n_{k,\downarrow})$ which decreases with increasing λ and finally vanishes in the localized phase [see Fig. 10(d)].

Next we investigate the momentum distribution in the regime $\Omega > \Omega_c$; similar to the noninteracting case, we see that in the delocalized regime the momentum distributions for both up and down spins are peaked at zero momentum, whereas in the localized phase they are peaked at finite momentum and other momentum modes get gradually occupied [see Figs. 12(a) and 12(b)]. Thus we conclude the the peak splitting of the momentum distribution of bosons is robust against weak on-site interaction between them.

[1] R. Nandkishore and D. A. Huse, Annu. Rev. Condens. Matter Phys. **6**, 15 (2015); E. Altman and R. Vosk, *ibid.* **6**, 383 (2015).

[2] A. Pal and D. A. Huse, Phys. Rev. B **82**, 174411 (2010); I. L. Aleiner, B. L. Altshuler, and G. V. Shlyapnikov, Nat. Phys. **6**, 900 (2010).

[3] M. Greiner, O. Mandel, T. Esslinger, T. W. Hnsch, and I. Bloch, Nature (London) **415**, 39 (2002); I. Bloch, J. Dalibard, and W. Zwerger, Rev. Mod. Phys. **80**, 885 (2008).

[4] M. Schreiber *et al.*, Science **349**, 842 (2015); P. Bordia, H. P. Lüschen, S. S. Hodgman, M. Schreiber, I. Bloch, and U. Schneider, Phys. Rev. Lett. **116**, 140401 (2016).

[5] S. S. Kondov, W. R. McGehee, W. Xu, and B. DeMarco, Phys. Rev. Lett. **114**, 083002 (2015).

[6] A. I. Goldman and R. F. Kelton, Rev. Mod. Phys. **65**, 213 (1993).

[7] R. Lifshitz, Rev. Mod. Phys. **69**, 1181 (1997).

[8] M. Quilichini, Rev. Mod. Phys. **69**, 277 (1997).

[9] S. Aubry and G. André, Ann. Isr. Phys. Soc. **3**, 133 (1980).

[10] C. Aulbach, A. Wobst, G. L. Ingold, P. Hänggi, and I. Varga, New J. Phys. **6**, 70 (2004); M. Modugno, *ibid.* **11**, 033023 (2009).

[11] S. Iyer, V. Oganesyan, G. Refael, and D. A. Huse, Phys. Rev. B **87**, 134202 (2013).

[12] X. Li, S. Ganeshan, J. H. Pixley, and S. Das Sarma, Phys. Rev. Lett. **115**, 186601 (2015).

[13] Y. Lahini, R. Pugatch, F. Pozzi, M. Sorel, R. Morandotti, N. Davidson, and Y. Silberberg, Phys. Rev. Lett. **103**, 013901 (2009).

[14] G. Roati *et al.*, Nature (London) **453**, 895 (2008).

[15] K. Singh, K. Saha, S. A. Parameswaran, and D. M. Weld, Phys. Rev. A **92**, 063426 (2015).

[16] G. Modugno, Rep. Prog. Phys. **73**, 102401 (2010); V. P. Michal, B. L. Altshuler, and G. V. Shlyapnikov, Phys. Rev. Lett. **113**, 045304 (2014); S. Ray, M. Pandey, A. Ghosh, and S. Sinha, New J. Phys. **18**, 013013 (2016).

[17] L. Fallani, J. E. Lye, V. Guarrera, C. Fort, and M. Inguscio, Phys. Rev. Lett. **98**, 130404 (2007); Chiara D'Errico *et al.*, *ibid.* **113**, 095301 (2014).

[18] M. White, M. Pasienski, D. McKay, S. Q. Zhou, D. Ceperley, and B. DeMarco, Phys. Rev. Lett. **102**, 055301 (2009); C. Meldgin, U. Ray, P. Russ, D. Chen, D. M. Ceperley, and B. DeMarco, Nat. Phys. **12**, 646 (2016).

[19] M. P. A. Fisher, P. B. Weichman, G. Grinstein, and D. S. Fisher, Phys. Rev. B **40**, 546 (1989); G. Roux, T. Barthel, I. P. McCulloch, C. Kollath, U. Schollwöck, and T. Giamarchi, Phys. Rev. A **78**, 023628 (2008); G. Roux, A. Minguzzi, and T. Roscilde, New J. Phys. **15**, 055003 (2013).

[20] R. Roth and K. Burnett, Phys. Rev. A **68**, 023604 (2003).

[21] Y.-J. Lin, R. L. Compton, K. Jimenez-Garcia, J. V. Porto, and I. B. Spielman, Nature (London) **462**, 628 (2011).

[22] J. Dalibard, F. Gerbier, G. Juzeliūnas, and P. Öhberg, Rev. Mod. Phys. **83**, 1523 (2011).

[23] S. Sinha and K. Sengupta, Europhys. Lett. **93**, 30005 (2011); S. Powell, R. Barnett, R. Sensarma, and S. Das Sarma, Phys. Rev. Lett. **104**, 255303 (2010); K. Saha, K. Sengupta, and K. Ray, Phys. Rev. B **82**, 205126 (2010).

[24] D. Jaksch and P. Zoller, New J. Phys. **5**, 56 (2003); E. J. Mueller, Phys. Rev. A **70**, 041603(R) (2004); K. Osterloh, M. Baig, L. Santos, P. Zoller, and M. Lewenstein, Phys. Rev. Lett. **95**, 010403 (2005); N. Goldman, A. Kubasiak, P. Gaspard, and M. Lewenstein, Phys. Rev. A **79**, 023624 (2009); I. B. Spielman, *ibid.* **79**, 063613 (2009).

[25] V. Galitski and I. B. Spielman, Nature (London) **494**, 49 (2013); N. Goldman, G. Juzeliūnas, P. Öhberg, and I. B. Spielman, Rep. Prog. Phys. **77**, 126401 (2014); T. Grass, K. Saha, K. Sengupta, and M. Lewenstein, Phys. Rev. A **84**, 053632 (2011).

[26] Y.-J. Lin, K. Jiménez-Garca, and I. B. Spielman, Nature (London) **471**, 83 (2011).

[27] Y. Li, G. I. Martone, and S. Stringari, in *Annual Review of Cold Atoms and Molecules* (World Scientific, Singapore, 2015), Vol. 3, Chap. 5, pp. 201–250.

[28] Y. Li, L. P. Pitaevskii, and S. Stringari, Phys. Rev. Lett. **108**, 225301 (2012).

[29] J. Radić, A. di Ciolo, K. Sun, and V. Galitski, Phys. Rev. Lett. **109**, 085303 (2012); W. S. Cole, S. Zhang, A. Paramekanti, and N. Trivedi, *ibid.* **109**, 085302 (2012).

[30] S. Mandal, K. Saha, and K. Sengupta, Phys. Rev. B **86**, 155101 (2012); S. Sinha, R. Nath, and L. Santos, Phys. Rev. Lett. **107**, 270401 (2011); Z. Cai, X. Zhou, and C. Wu, Phys. Rev. A **85**, 061605(R) (2012).

[31] H. M. Hurst, J. H. Wilson, J. H. Pixley, I. B. Spielman, and S. S. Natu, Phys. Rev. A **94**, 063613 (2016).

[32] G. I. Martone, T. Ozawa, C. Qu, and S. Stringari, Phys. Rev. A **94**, 043629 (2016); Z. Chen and Z. Liang, *ibid.* **93**, 013601 (2016).

[33] Y. Cheng, G. Tang, and S. K. Adhikari, Phys. Rev. A **89**, 063602 (2014).

[34] L. Zhou, H. Pu, and W. Zhang, Phys. Rev. A **87**, 023625 (2013).

[35] M. Kohmoto and D. Tobe, Phys. Rev. B **77**, 134204 (2008).

[36] D. Tobe, M. Kohmoto, M. Sato, and Y. S. Wu, Phys. Rev. B **75**, 245203 (2007).

[37] Y.-C. Zhang, Z.-Q. Yu, T. K. Ng, S. Zhang, L. Pitaevskii, and S. Stringari, Phys. Rev. A **94**, 033635 (2016).

[38] M. E. Fisher, M. N. Barber, and D. Jasnow, Phys. Rev. A **8**, 1111 (1973).

[39] A. J. Leggett, Rev. Mod. Phys. **73**, 307 (2001).

[40] J. Simon, W. S. Bakr, R. Ma, M. E. Tai, P. M. Preiss, and M. Greiner, Nature (London) **472**, 307 (2011).

[41] T. D. Kuhner, S. R. White, and H. Monien, Phys. Rev. B **61**, 12474 (2000).

[42] B. Pandey, S. Sinha, and S. K. Pati, Phys. Rev. B **91**, 214432 (2015).

[43] G. Lenz and F. Haake, Phys. Rev. Lett. **65**, 2325 (1990); **67**, 1 (1991); S. Schierenberg, F. Bruckmann, and T. Wettig, Phys. Rev. E **85**, 061130 (2012).

[44] M. V. Berry and M. Robnik, J. Phys. A: Math. Gen. **17**, 2413 (1984); K. Ź yczkowski, M. Lewenstein, M. Kuś, and F. Izrailev, Phys. Rev. A **45**, 811 (1992).

[45] Y. Y. Atas, E. Bogomolny, O. Giraud, and G. Roux, Phys. Rev. Lett. **110**, 084101 (2013).

[46] F. Haake, *Quantum Signatures of Chaos*, Springer Science and Business Media (Springer, Berlin/Heidelberg, 2013), Vol. 54.

[47] F. M. Izrailev, Phys. Rep. **196**, 299 (1990); V. Zelevinsky, B. A. Brown, N. Frazier, and M. Horoi, *ibid.* **276**, 85 (1996).

[48] J. Pipek and I. Varga, Phys. Rev. A **46**, 3148 (1992); P. Jacquod and I. Varga, Phys. Rev. Lett. **89**, 134101 (2002).

[49] P. Bordia, H. Lüschen, U. Schneider, M. Knap, and I. Bloch, Nat. Phys. **13**, 460 (2017).

[50] J. Stenger, S. Inouye, D. M. Stamper-Kurn, H. J. Miesner, A. P. Chikkatur, and W. Ketterle, Nature (London) **396**, 345 (1998).

[51] D. S. Petrov, D. M. Gangardt, and G. V. Shlyapnikov, J. Phys. IV France **116**, 5 (2004).